Section S1. Contact-angle theory and HMDS surface reaction

Purpose: This section provides the theoretical background of contact-angle analysis and the chemical mechanism of HMDS surface modification, which complement the experimental results shown in Fig. 2 of the main text.

S1.1 Contact-angle equilibrium

The equilibrium contact angle (θ) of a droplet on a solid surface is governed by the interfacial tensions at the solid–liquid–gas boundary. According to **Young's equation**:

$$cos\theta = \frac{(\gamma SG - \gamma SL)}{\gamma LG} \qquad [1]$$

where γSG, γSL, and γLG represent the interfacial tensions at the solid-gas, solid-liquid, and liquid-gas interfaces, respectively. A smaller contact angle (θ) corresponds to higher solid surface energy (γSG), leading to enhanced liquid spreading and increased hydrophilicity. Conversely, a larger contact angle indicates lower surface energy, which suppresses liquid spreading and promotes hydrophobicity.

S1.2 Reaction mechanism of HMDS surface functionalization

Hexamethyldisilazane (HMDS) reacts with surface hydroxyl (–OH) groups on SiO_2 through a condensation reaction, forming Si–O–Si bonds and releasing ammonia.

The reaction can be expressed as:

$$[(CH_3)_3Si]_2NH + Si\text{-}OH \rightarrow (CH_3)_3Si\text{-}O\text{-}Si + NH_3 \uparrow$$

This substitution replaces polar hydroxyl groups with non-polar methyl groups, effectively reducing surface polarity and increasing the contact angle, resulting in a stable hydrophobic surface suitable for localized droplet confinement and region-selective biofunctionalization.

Section S2. Stability of (HMDS) Hydrophobic Modification

To further evaluate the robustness of the surface chemical treatment, the hydrophobicity of the ~~HDMS~~ HMDS-modified GFET device was examined one month after processing. As shown in Figure S1, the contact angle measurement remains consistent with the initial characterization (~83°), indicating that the hydrophobic modification is stable over a long period of time. This result demonstrates that the HMDS layer is not only effective immediately after treatment but also durable, which is critical for reliable device storage and subsequent biofunctionalization.

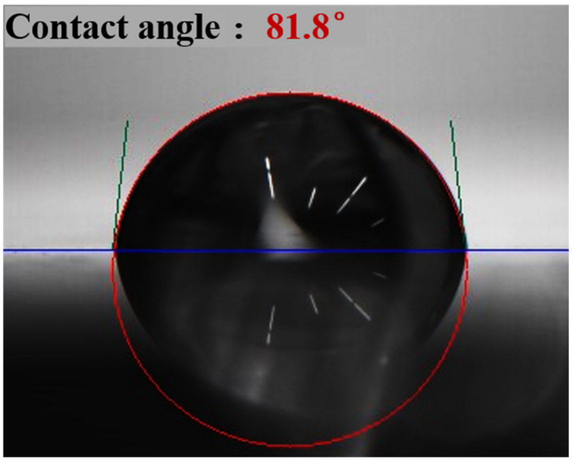

Figure S1. Contact angle measurement of the GFET device surface one month after HDMS treatment

Section S3. Droplet Separation and stability during Functionalization

During the aptamer functionalization process, incubation typically lasts for 3 h. To verify that the droplets remain spatially separated within each functionalization region during this time, we conducted a time-dependent comparison. As shown in Figure S2, the droplets deposited at 0 min and after 3 h of incubation remain well confined in their designated regions without merging. This confirms that the HDMS-induced hydrophobic partitioning is effective in maintaining spatial isolation throughout the functionalization process, thereby ensuring the feasibility of multi-target modification on a single GFET chip.

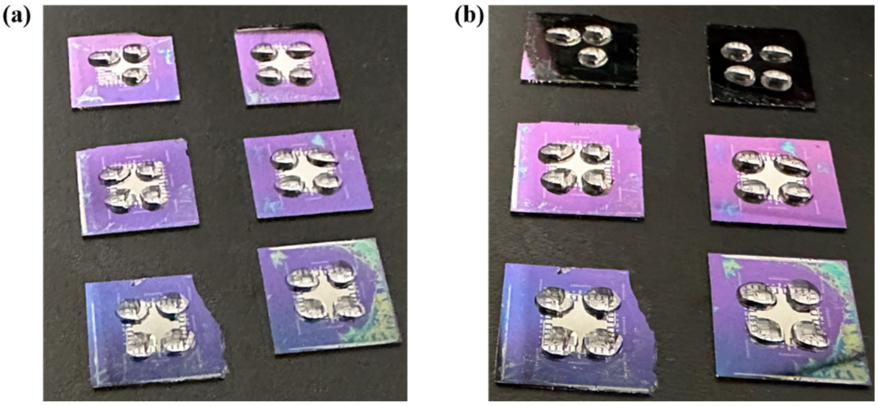

Figure S2. Optical images of droplet distribution on multi-chip GFET devices at (a) 0 min and (b) after 3 h of incubation.

Table S1. Dirac-point voltage shifts (ΔV_{cnp}) of the dual-aptamer GFET upon single-target $A\beta_{42}$ exposure at various concentrations

Data were collected from two independent chips, each comprising four sensing regions with four devices per region. Two types of aptamers (hsa-miR-125b and $A\beta_{42}$) were functionalized on separate regions of the same chip, yielding at least 13 valid devices per aptamer type ($n \geq 13$).

Mean ± SD values are shown, and statistical differences were evaluated using two-tailed Welch's *t*-tests ($p < 0.05$).

Concentration (M)	ΔV_{cnp} (V ± SD) hsa-miR-125b region	ΔV_{cnp} (V ± SD) $A\beta_{42}$ region	p-value
1.00×10^{-15}	0.010 ± 0.016	0.031 ± 0.008	0.004
1.00×10^{-12}	0.020 ± 0.006	0.070 ± 0.004	< 0.001
1.00×10^{-9}	0.023 ± 0.012	0.156 ± 0.005	< 0.001
1.00×10^{-8}	0.025 ± 0.005	0.207 ± 0.027	< 0.001
1.00×10^{-7}	0.033 ± 0.007	0.232 ± 0.012	< 0.001

(Data represent mean ± standard deviation of ΔV_{cnp} values obtained from ⩾13 devices per aptamer type, measured across two dual-aptamer chips.)

Table S2. Dirac-point voltage shifts ((ΔV_{cnp}) of the dual-aptamer GFET upon single-target hsa-miR-125b exposure at various concentrations

Data were collected from two independent dual-aptamer chips, each containing four sensing regions with four devices per region. Two types of aptamers (hsa-miR-125b and $A\beta_{42}$) were functionalized on separate regions of the same chip, yielding at least 13 valid devices per aptamer type ($n \geqslant 13$). Mean ± SD values are shown, and statistical differences were analyzed using two-tailed Welch’s t-tests ($p < 0.05$).

Concentration (M)	ΔV_{cnp} (V ± SD) hsa-miR-125b region	ΔV_{cnp} (V ± SD) $A\beta_{42}$ region	p-value
1.00×10^{-15}	0.023 ± 0.011	0.013 ± 0.004	0.010
1.00×10^{-12}	0.034 ± 0.010	0.013 ± 0.009	< 0.001
1.00×10^{-9}	0.072 ± 0.008	0.026 ± 0.005	< 0.001
1.00×10^{-8}	0.091 ± 0.013	0.023 ± 0.004	< 0.001
1.00×10^{-7}	0.143 ± 0.005	0.033 ± 0.004	< 0.001

(Data represent mean ± standard deviation of ΔV_{cnp} values obtained from ⩾13 devices per aptamer type, measured across two dual-aptamer chips.)

Tables S1 and S2 together confirm the orthogonal recognition of $A\beta_{42}$ and hsa-miR-125b in the dual-aptamer GFET biosensor.